Human Molecular Genetics, 2019, Vol. 28, No. 11 1894–1904

doi: 10.1093/hmg/ddz030
Advance Access Publication Date: 28 January 2019
General Article

GENERAL ARTICLE

GBA haploinsufficiency accelerates alpha-synuclein pathology with altered lipid metabolism in a prodromal model of Parkinson's disease

Masashi Ikuno[1], Hodaka Yamakado[1,*], Hisako Akiyama[2], Laxmi Kumar Parajuli[3], Katsutoshi Taguchi[4], Junko Hara[1], Norihito Uemura[1], Yusuke Hatanaka[1], Katsumi Higaki[5], Kousaku Ohno[6], Masaki Tanaka[4], Masato Koike[3], Yoshio Hirabayashi[2] and Ryosuke Takahashi[1,*]

[1]Department of Neurology Kyoto University Graduate School of Medicine, Kyoto 606-8507, Japan, [2]Laboratory for Molecular Membrane Neuroscience, RIKEN Brain Science Institute, Saitama 351-0198, Japan, [3]Department of Cell Biology and Neuroscience, Juntendo University Graduate School of Medicine, Tokyo 113-0033, Japan, [4]Department of Anatomy and Neurobiology, Graduate School of Medical Science, Kyoto Prefectural University of Medicine, Kyoto 602-8566, Japan, [5]Division of Functional Genomics, Research Center for Bioscience and Technology, Faculty of Medicine, Tottori University, Tottori 680-8550, Japan and [6]Sanin Rosai Hospital, Tottori 683-0002, Japan

*To whom correspondence should be addressed at: Hodaka Yamakado, Department of Neurology, Kyoto University Graduate School of Medicine, 54 Shogoin Kawahara-cho, Sakyo-ku, Kyoto 606-8507, Japan. Tel: +81-75-751-3767; Fax: +81-75-761-9780; Email: yamakado@kuhp.kyoto-u.ac.jp and Ryosuke Takahashi, Department of Neurology, Kyoto University Graduate School of Medicine, 54 Shogoin Kawahara-cho, Sakyo-ku, Kyoto 606-8507, Japan. Tel: +81-75-751-3770; Fax: +81-75-761-9780; Email: ryosuket@kuhp.kyoto-u.ac.jp

Abstract

Parkinson's disease (PD) is characterized by dopaminergic (DA) cell loss and the accumulation of pathological alpha synuclein (asyn), but its precise pathomechanism remains unclear, and no appropriate animal model has yet been established. Recent studies have shown that a heterozygous mutation of *glucocerebrosidase* (*gba*) is one of the most important genetic risk factors in PD. To create mouse model for PD, we crossed asyn Bacterial Artificial Chromosome transgenic mice with *gba* heterozygous knockout mice. These double-mutant (*dm*) mice express human asyn in a physiological manner through its native promoter and showed an increase in phosphorylated asyn in the regions vulnerable to PD, such as the olfactory bulb and dorsal motor nucleus of the vagus nerve. Only *dm* mice showed a significant reduction in DA cells in the substantia nigra pars compacta, suggesting these animals were suitable for a prodromal model of PD. Next, we investigated the *in vivo* mechanism by which GBA insufficiency accelerates PD pathology, focusing on lipid metabolism. *Dm* mice showed an increased level of glucosylsphingosine without any noticeable accumulation of glucosylceramide, a direct substrate of GBA. In addition, the overexpression of asyn resulted in decreased GBA activity in mice, while *dm* mice tended to show an even further decreased level of GBA activity. In conclusion, we created a novel prodromal mouse model to study the disease pathogenesis and develop novel therapeutics for PD and also revealed the mechanism by which heterozygous *gba* deficiency contributes to PD through abnormal lipid metabolism under conditions of an altered asyn expression *in vivo*.

Received: September 13, 2018. **Revised:** January 21, 2019. **Accepted:** January 23, 2019

Introduction

Parkinson's disease (PD) is the most common movement disorder and is pathologically characterized by the progressive dopaminergic (DA) cell loss and the formation of Lewy bodies (LB). Thus far, the precise pathomechanism of PD has been unclear, and no appropriate animal model that faithfully recapitulates the clinical course and neuropathology has been available. Alpha synuclein (asyn) remains an attractive target candidate for PD therapy, as it is a major component of LB and its expression is upregulated in the brains of PD patients. Genetic studies have also shown that multiplications (duplication and triplication) of asyn are responsible for familial PD, which shares many clinical and pathological features with idiopathic PD (1,2,3). In addition, single-nucleotide polymorphisms (SNPs) of asyn were found to be genetic risk factors for idiopathic PD (4,5). These findings suggest that the quantitative change in the asyn expression is an important factor for the development of PD, suggesting that the overexpression of asyn may be a reasonable strategy for creating a mouse model of PD.

The most successful model of PD induction by asyn overexpression is a *Drosophila* model, which shows DA cell loss associated with asyn inclusion and age-dependent locomotion defects (6). However, flies lack their own asyn and differ markedly from humans with regard to anatomy, physiology and genetics. A mammalian model is therefore needed in order to investigate the disease pathogenesis and test novel therapeutics for human PD patients in a preclinical phase. A mouse model is ideal in terms of cost-effectiveness. The most widely used asyn-overexpressing mouse model is A53T human asyn transgenic mice with prion promotor (7). These animals show a progressive asyn pathology via strong exogenous asyn expression, but this expression is ectopic, and the mice do not show selective DA cell loss associated with the accumulation of asyn. We previously generated wild-type (*wt*) human asyn bacterial artificial chromosome (BAC) transgenic (*SNCA Tg/Tg*) mice that harbor the entire human asyn gene and its gene expression regulatory regions and mimic human PD with asyn multiplication. Although these mice exhibited an abnormal behavior such as a decrease in anxiety-like behavior, they also failed to show any obvious loss of DA cells or motor symptoms (8).

In recent years, the heterozygous mutation of *glucocerebrosidase* (*gba*), whose homozygous mutations are responsible for Gaucher's disease, was reported to be an important genetic risk factor for PD (9). Although the homozygous mutation of *gba* results in the accumulation of glucosylceramide (GlcCer) as well as asyn and also promote asyn pathology in Gaucher's disease cellular and mouse models (10,11,12), the heterozygous *gba* mutation *per se* is not regarded as pathogenic but is suspected to accelerate PD pathology *in vivo* by as-yet-unidentified mechanisms.

In the present study, we crossbred *SNCA Tg/Tg* mice with *gba* heterozygous knockout (*gba* +/−) mice using two genetic risk factors to create a relevant mouse model for PD. These mice are also useful for investigating how heterozygous *gba* mutations contribute to the PD pathology under conditions of an altered asyn expression *in vivo*.

Results

Generation of a prodromal mouse model for PD

The *SNCA Tg/Tg* mice used in this study have previously been described (8). The transgenic construct harbors the 5′- and 3′-flanking regions of the asyn gene which presumably contains gene expression regulatory regions (Fig. 1). We crossed these *SNCA Tg/Tg* mice with *gba* +/− mice to generate *dm* mice.

Asyn expression in *dm* mouse brain

In *dm* mice, transgenic asyn was highly expressed in the olfactory bulb (Ob)/ tubercle, cerebral cortex, hippocampus, striatum and substantia nigra pars compacta (SNpc) by its endogenous promoter (Fig. 2A). Because asyn is reported to be involved in presynaptic neurotransmitter release (13), suggesting its presynaptic expression, we also examined the locus of asyn expression by co-staining brain sections with asyn and vGluT-1 antibody. Similar to that in *wt* mice, asyn was expressed mainly at the vGluT-1-positive excitatory synapse in *dm* mice (Fig. 2B).

Behavioral phenotype of *dm* mice

In a behavioral analysis, *dm* mice did not show the typical motor phenotype of PD, such as hypoactivity. Quite the opposite, in an open field (OF) test, *dm* mice showed hyperactivity and an increased center time, both of which have previously been reported in *SNCA Tg/Tg* mice (8); this finding was interpreted to reflect decreased anxiety (Supplementary Material, Fig. S1A). Because cognitive decline is common in patients with asyn multiplication, especially in asyn triplication cases, we performed the Barnes maze test as a readout of the cognitive ability. No obvious cognitive impairment was observed in *dm* mice (Supplementary Material, Fig. S1B).

The pathological asyn accumulation in vulnerable brain regions in PD

Recent pathological studies using post-mortem brains have shown that the formation of Lewy pathology (LP), especially in the lower brainstem and the Ob, antedates motor symptoms in PD (14). Most of the asyn in LP is phosphorylated at serine 129, and phosphorylated asyn (phospho-asyn) has been recognized as a reliable marker with high sensitivity and specificity for LP in PD (15).

We examined the distribution of phospho-asyn using its specific antibody in *dm* mice, with a focus on the early-stage and vulnerable regions in PD. *Dm* mice highly expressed phospho-asyn in specific regions, such as the Ob and dorsal nucleus of the vagus nerve, where LP appears in the early stage of PD (Fig. 3). We also quantified the level of total and phospho-asyn expression using an immunoblot analysis. Among the four genotypes (*wt*, *gba* +/−, *SNCA Tg/Tg*, *dm*), asyn was mildly overexpressed in the transgenic group to the same extent as in *SNCA Tg/Tg* mice, but the level of phospho-asyn was significantly increased in *dm* mice compared with that in *SNCA Tg/Tg* mice (Fig. 4). Next, to examine whether or not asyn forms aggregates, we performed a pre-embedding electron microscopic analysis of asyn in the Ob. Immunogold was found to be diffusely localized, without any obvious clustering (Supplementary Material, Fig. S3). However, phospho-asyn and LAMP2 were co-localized and accumulated in enlarged dot-like structures, suggestive of the defective lysosomal turnover and dysfunction of the autophagy-lysosomal system (Supplementary Material, Fig. S2).

Mild DA cell loss in the SNpc in *dm* mice

Since DA cell loss in SNpc is a characteristic phenotype of PD, we counted the number of tyrosine hydroxylase (TH)-positive

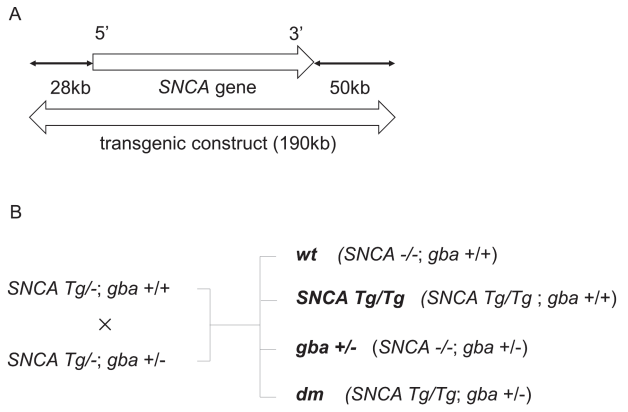

Figure 1. Generation of double-mutant (*dm*) mice (*SNCA Tg/Tg*; *gba* +/−). (**A**) The transgenic construct of *SNCA Tg/Tg* mice contains the human asyn gene and its 28-kb 5′- and 50-kb 3′-flanking regions, which enable the native expression of human asyn by its gene expression regulatory elements in mice. (**B**) *dm* mice (*SNCA Tg/Tg*; *gba* +/−) were generated by crossing mice (*SNCA Tg/Tg*; *gba* +/−) with each other.

cells in SNpc and found that the number was decreased only in *dm* mice (Fig. 5; Supplementary Material, Fig. S4). To assess the pathological changes associated with DA neurodegeneration, we performed toluidine blue staining of semi-thin slice sections of *dm* mice. Shrinking neurons with an increased intensity signal, which is suggestive of 'dark cell' degeneration, were observed in SNpc of *dm* mice (Fig. 6A). Electron microscopy (EM) inspection of ultra-thin sections revealed that the degenerating neurons with a high electron density were surrounded by electro-lucent processes that were possibly derived from astrocytes. Furthermore, the accumulation of mitochondria and vacuolation of the Golgi apparatus were visible in the perikarya in *dm* mice (Fig. 6B, C.). These findings of shrinking neurons loosely surrounded by astrocytes and not engulfed by phagocytic cells as well as the vacuolation of the Golgi apparatus were also reported in a Huntington's disease mouse model (16) and are thought to be common pathological findings in slowly progressive neurodegenerative conditions.

Investigation of the *in vivo* mechanisms of GBA heterozygous insufficiency contributing to PD

To investigate the relationship between the expression of asyn and the GBA activity, we measured the GBA enzymatic activity and performed a glycolipids analysis including GlcCer, a substrate of GBA.

The activity of GBA in *dm* mice

Interestingly, the GBA activity of the whole brain lysate was significantly decreased in *SNCA Tg/Tg* mice without a *gba* mutation. Furthermore, a decreasing trend was noted in *dm* mice compared with *gba* +/− mice (Fig. 7A). The decreased GBA activity by asyn overexpression and the tendency toward further decreased activity of GBA in *dm* mice were observed in the cerebral cortex, where asyn was highly expressed; however, these findings were not obvious in the cerebellum, where the expression of asyn was low (Supplementary Material, Fig. S5).

The accumulation of glucosylsphingosine in *dm* mice

Next, we performed a glycolipids analysis by hydrophilic interaction chromatography (HILIC)-electrospray ionization tandem mass spectrometry (ESI-MS/MS), which has a high resolution capable of distinguishing GlcSph from galactosylsphingosine. No significant difference was noted in the levels of ceramide, sphingosine or GlcCer between *wt* and *dm*, with only the level of GlcSph significantly increased in *dm* mice (Fig. 7; Supplementary Material, Fig. S6). For comparison, we also measured the GBA activity and the level of glycolipids in mice with *gba D409V* homozygous mutation (*gba D409V/D409V*), a mouse model for Gaucher's disease that showed a GBA activity of <10% in *wt* mice (17). Again, the accumulation of GlcSph was more profound than that of GlcCer in *gba D409V/D409V* mice (Supplementary Material, Fig. S6).

Discussion

In the present study, we crossed *SNCA Tg/Tg* mice with *gba* +/− mice to generate *dm* mice that can be used to perform a mechanistic analysis of the link between heterozygous mutation of *gba* and PD. Although both loss-of-function and gain-of-function have been proposed to be the underlying mechanisms of GBA-associated PD (11,18), the presence of null mutations in GBA-associated PD patients and a positive correlation between the risk of parkinsonism and the severity of the decrease in enzymatic activity in *GBA* mutations suggest that loss-of-function mechanisms contribute in part to PD pathology (19). This study focused on the loss-of-function mechanism of *gba* mutations contributing to PD using *gba* heterozygous knockout mice.

Idiopathic PD is pathologically characterized by DA cell loss and the accumulation of asyn in specific brain regions. Most of the mouse models that show the accumulation of asyn do not exhibit DA cell loss, and the distribution of asyn aggregates in these models is different from that in PD brains, as asyn is ectopically overexpressed by potent exogenous promoters. In the present study, we used asyn BAC transgenic (tg) mice mildly overexpressing asyn through its native promoter to generate *dm* mice.

The degree of DA cell loss was mild, and the typical motor phenotype of PD was not seen in *dm* mice. Instead, these mice exhibited hyperlocomotion in an OF test, which has also been observed in *SNCA Tg/Tg* mice (8) and other asyn tg mice, such as A53T mutant asyn tg mice driven by the prion promoter (20). This behavioral phenotype is not necessarily inconsistent with mild DA loss, as motor symptoms generally lag profound DA cell loss (at least 50% loss in PD).

Recent pathological and experimental studies have suggested that there are two pathways for the development of asyn pathology in PD brains: one ascending from the dorsal motor nuclei of the vagal nerve (DMV) to the midbrain and cerebral cortex, and the other starting from the Ob and spreading to the limbic system and cerebral cortex (14). Although most of the structures immunopositive for phospho-asyn show a punctate pattern, suggestive of their presynaptic localization, in the DMV and Ob, phospho-asyn was found to be accumulated in cell bodies, possibly recapitulating the early pathological changes in PD. However, the limitation of this mouse model is that only aged *dm* mice (16–18 months old) showed DA neurodegeneration and asyn pathology, so it cannot be used as a prodromal PD mouse model, especially in preclinical studies. Nevertheless, this model is still useful for examining the very early changes in the preclinical stages leading to DA neuronal loss by aging.

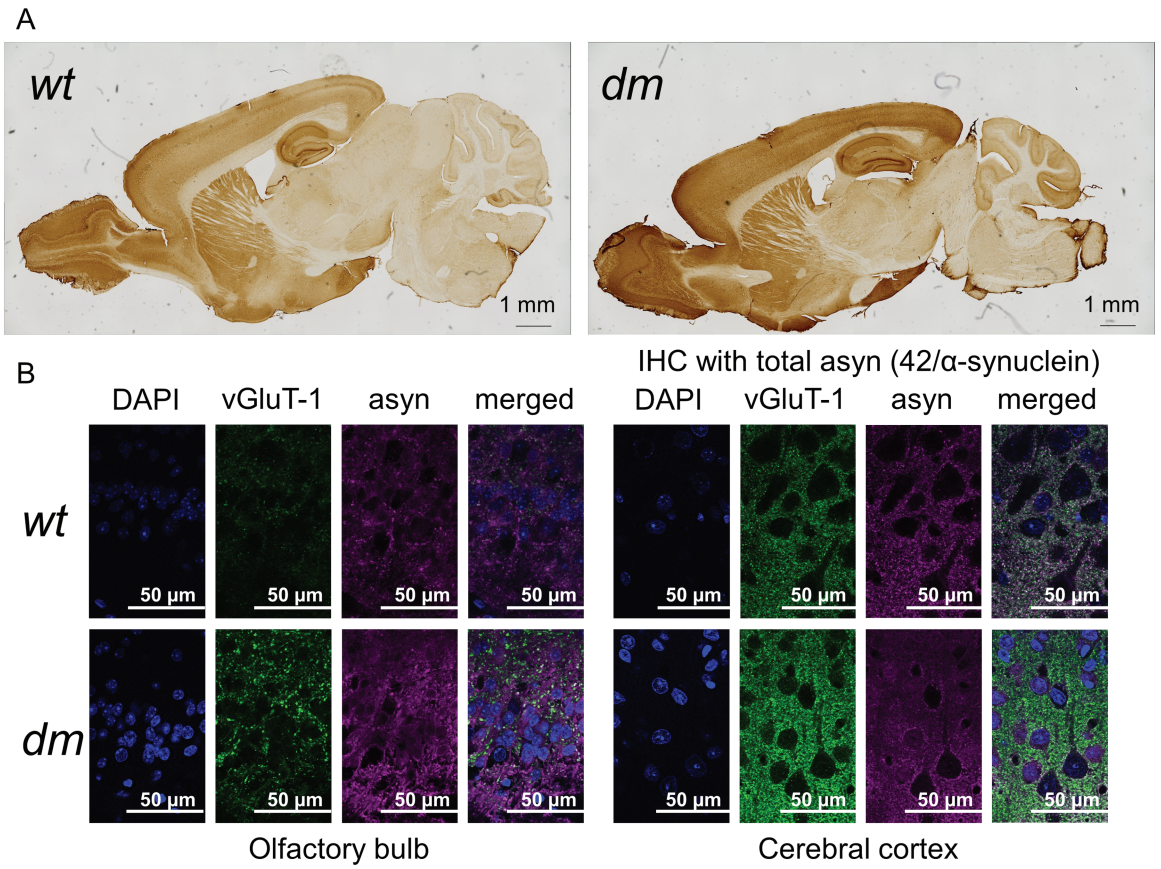

Figure 2. Expression pattern of asyn in *wt* and *dm* mice. (**A**) Immunohistochemical staining of sagittal sections of whole brains with total (mice and human) asyn revealed that the total asyn was expressed mainly in the Ob, cerebral cortex, striatum and substantia nigra in 24-month-old mice of both genotypes. (**B**) The synaptic expression patterns of asyn. Asyn was expressed mainly at the vGluT1-positive excitatory synapse in 18-month-old *wt* as well as *dm* mice. The bars indicate 50 μm. *wt*: wild type, *dm*: double-mutant (*SNCA Tg/Tg*; *gba* +/−).

To investigate the pathomechanisms underlying the accumulation of pathogenic asyn and DA cell loss in *dm* mice, we focused on the interaction between the GBA activity and the expression of asyn. The GBA activity was shown to be decreased in total brains of *SNCA Tg/Tg* mice. We speculated that the GBA activity was directly affected by the mild overexpression of asyn, as this phenomenon was seen in the cortex, where asyn is highly expressed, but not in the cerebellum, where asyn is poorly expressed. As asyn is highly expressed in a specific type of cells in contrast to the ubiquitous expression of GBA, the GBA activity of asyn-expressing cells may have been further decreased to an extent that caused the asyn accumulation, as was the case with Gaucher's disease. This idea is consistent with the findings of previous studies showing that asyn inhibits lysosomal trafficking of GBA and decreases its activity, leading to the formation of a vicious bidirectional loop between asyn accumulation and a reduced GBA activity (21), and that such reduced GBA activity prolongs the degradation time of asyn *in vivo* (22).

We then measured the levels of glycolipid associated with GBA to investigate the effect of heterozygous mutation of *gba* and an altered asyn expression. *Dm* mice showed the accumulation of GlcSph, which is the deacylated form of GlcCer and has been reported to be accumulated in Gaucher's disease patients (23). Although the increase in GlcSph was mild compared to that previously reported in mice with *gba* homozygous mutations (12), the increase may be more marked if specifically measured in cells expressing asyn.

Although there was no significant difference in GlcCer level between wt and mutants, GlcCer was significantly increased in both SNCA Tg/Tg and gba +/− by Dunnett's multiple comparison test using *dm* as a control (data not shown). Although it is difficult to find the reason for this unexpected result, there could be an altered metabolism in dm, for example, an increased deacylation of GlcCer into GlcSph.

We further performed a glycolipids analysis in *gba D409V/D409V* mice that shows more reduced GBA activity compared with *gba* +/− mice. Although both GlcCer and GlcSph were accumulated in *gba D409V/D409V* mice, GlcSph showed a more marked increase, suggesting that it is a more sensitive maker of decreased GBA activity than GlcCer. While increased levels of sphingosine in gba +/− and SNCA Tg/Tg mice were observed and might have canceled each other out in *dm* mice, their significance was unclear, as such changes were not observed in gba D409V/D409V mice, which showed a reduced GBA activity and an increased accumulation of GlcSph and GlcCer.

In recent years, it was reported that glycolipids such as GlcSph and GlcCer promoted the pathological formation of asyn (24), and *dm* mice actually showed increased levels of phospho-asyn compared to *SNCA Tg/Tg* mice despite the expression of total asyn being equivalent between these genotypes. A heterozygous mutation of *gba* may have caused the increased

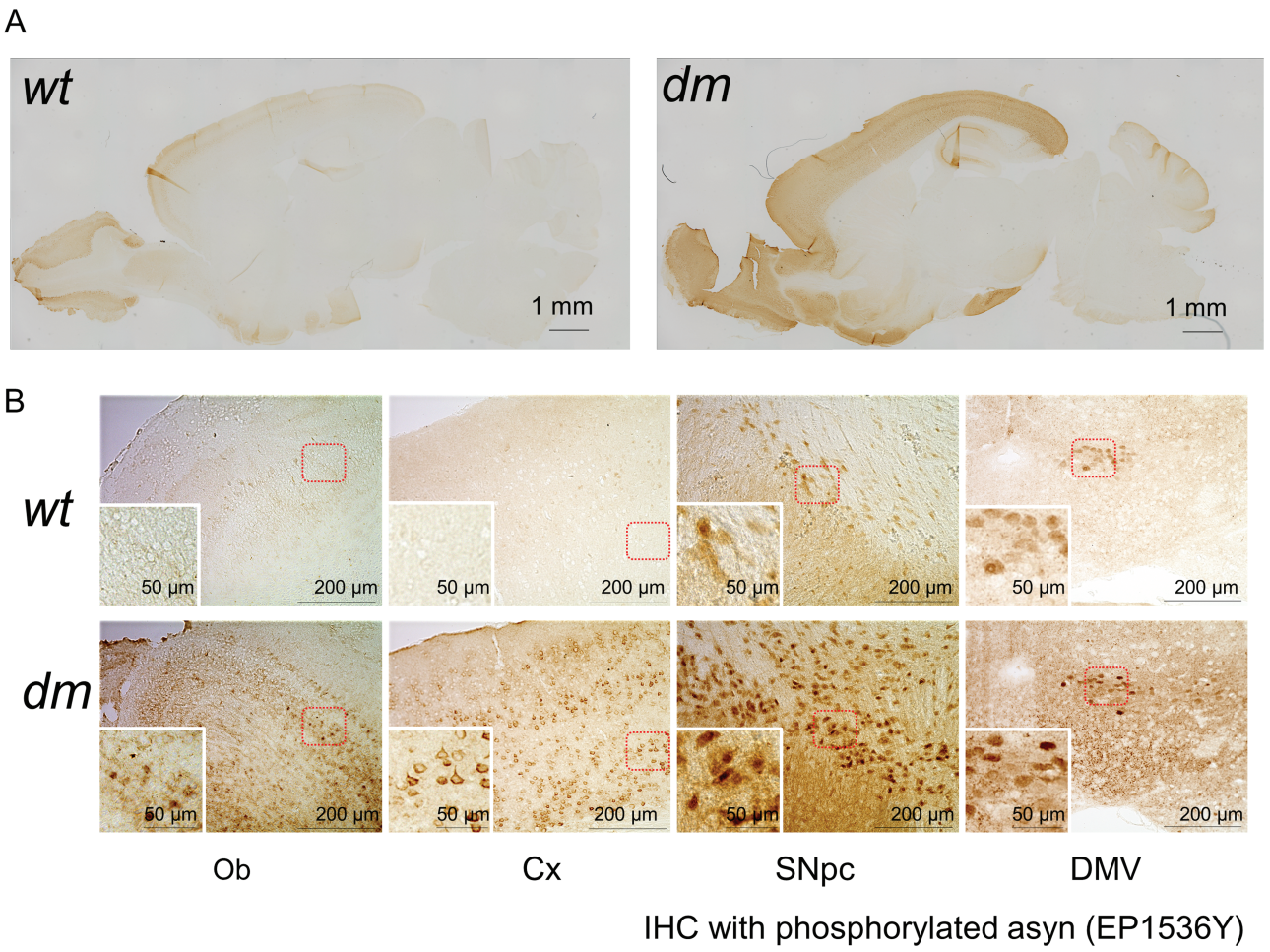

Figure 3. Distribution of phospho-asyn in vulnerable regions in Parkinson's disease in *dm* mice. (**A**) Immunohistochemical staining of sagittal sections of whole brains with phospho-asyn revealed that it is highly expressed in 24-month-old *dm* mice. (**B**) Immunohistochemical staining with phospho-asyn focused on the vulnerable regions in Parkinson's disease. Phospho-asyn was highly accumulated in the Ob and cerebral cortex as well as in specific nuclei in the brainstem, such as the SNpc and DMV in 18-month-old *dm* mice. Note the strong phospho-asyn immunoreactivity in the cell bodies of the Ob, SNpc and DMV (vulnerable regions in the early stage of Parkinson's disease), in *dm* mice. *wt*: wild type, *dm*: double-mutant (*SNCA Tg/Tg*; *gba* +/−). Ob: olfactory bulb, Cx: cortex, SNpc: substantia nigra pars compacta, DMV: dorsal motor nucleus of the vagus nerve.

pathological concentration of asyn through the accumulation of GlcSph under conditions of a mildly increased level of asyn.

A number of reports have described the metabolic abnormalities induced by *gba* homozygous mutations that cause Gaucher's disease, but few have described those induced by heterozygous *gba* mutations, which are implicated in PD. A recent study by Tayebi *et al.* (25) also showed that GBA haploinsufficiency in A53T asyn mice influenced the disease onset and course, but no abnormalities in the GBA-related lipid metabolism have yet been observed. Differences in the asyn tg mice used in the study (prion promoter-driven tg versus BAC tg) may account for the different results obtained in the lipid metabolism. Our study unequivocally demonstrated for the first time that even heterozygous mutations of *gba* influence the lipid metabolism and contribute to the pathological accumulation of asyn under conditions of a mildly increased level of asyn.

In the present study, we created a novel prodromal PD mouse model using two genetic risk factors and clarified the mechanism by which heterozygous *gba* deficiency contributes to PD through abnormal lipid metabolism under conditions of an altered asyn expression *in vivo*. Given that the GBA activity is reported to be decreased in PD brains (26), and its decrease is enhanced by the increased expression of asyn, as shown in the present study, augmenting the GBA activity or reducing the asyn expression appears to be a potential strategy for treating PD, regardless of the *gba* mutation status.

Materials and Methods

Animals

Mice were kept in a temperature-controlled facility on a 12 h light/dark cycle with free access to food and water. The generation of *SNCA Tg/Tg* mice has been described elsewhere (8). *gba* +/− mice (strain name: B6.129S6-Gba < tm1Nsb>/J, stock number: 003321) (27) and *gba D409V/D409V* (strain name: C57BL/6 N-Gbatm1.1 Mjff/J, stock number: 019106, Information obtained from the Jackson Laboratory, Unpublished: MGI: J: 101977) were purchased from the Jackson Laboratory (Bar Harbor, ME, USA). Transgenic and knockout mice were maintained on a B6/J background. Polymerase chain reaction (PCR) for human SNCA, mouse GBA and the mouse IL2 gene were performed with each of the following primer sets: SNCA fw 5′-ACTTGCTAGGCCACCTGAGA-3′, SNCA rv

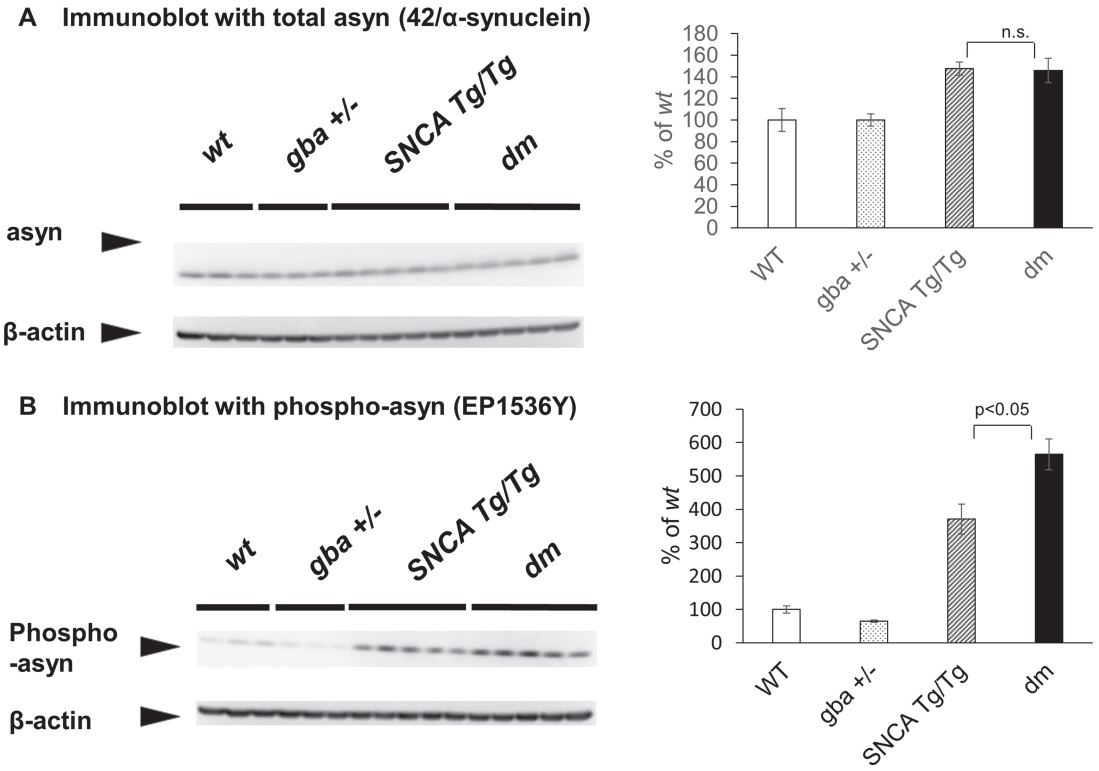

Figure 4. A quantitative analysis of the total and phospho-asyn expression. (**A**) An immunoblot analysis of the total asyn in the cerebral cortex of 16- to 18-month-old mice showed that asyn was mildly overexpressed in the asyn transgenic group, but there was no significant difference between *SNCA* Tg/Tg and *dm* mice. $n = 3$ for *wt* and *gba* +/−, and $n = 5$ for *SNCA* Tg/Tg and *dm* mice. (**B**) An immunoblot analysis of phospho-asyn in the cerebral cortex of 16- to 18-month-old mice. The expression of phospho-asyn was significantly increased in the *dm* mice compared to the *SNCA* Tg/Tg mice ($P < 0.05$). P-asyn: phospho-asyn. $n = 3$ for *wt* and *gba* +/−, and $n = 5$ for *SNCA* Tg/Tg and *dm* mice. *wt*: wild type, *dm*: double-mutant (*SNCA* Tg/Tg; *gba* +/−). The bars indicate mean ± SEM values. The significance of changes was analyzed by a one-way analysis of variance, followed by Tukey's multiple comparison, with $P < 0.05$ deemed significant.

5′-ATGCCAGGTGTTTGGAAAAG-3′; GBA fw 5′-ACACGACCACAAC TGCAGAG-3′, GBA rv 5′-CGTAACTGGATGGACGGACTG-3′, GBA KO 5′-GCTATCAGGACATAGCGTTGG-3′; IL2 fw: 5′-ATAAATTGCCTCCC ATGCTGA-3′, IL2 rv: 5′ -GATGCGAGCTGCATGCTGTA-3′. Electrophoresis on a 2% (w/v) polyacrylamide gel was then performed. Real-time PCR for human SNCA and the mouse IL2 gene were performed with the following primer sets: SNCA fw: 5′-GGCTGATGCCAACAAGCTGT-3′, SNCA rw: 5′-GTGGAATTTCGC ACAAACCCT-3′; IL2 fw: 5′-ATAAATTGCCTCCCATGCTGA-3′, IL2 rv: 5′-GATGCGAGCTGCATGCTGTA-3′). All of the experimental protocols were approved by the Ethics Committee for Animal Experiments of Kyoto University.

Open field test

The OF test was assessed using an OF instrument (Accuscan Instruments, Columbus, OH, USA) as previously described (28). In brief, the mice were placed at the center of an OF (40 × 40 × 30 cm), and the total walking distance, the time spent in the center area, the vertical activity and the stereotypic movements were recorded for 2 h.

Barnes maze test

The Barnes maze test was performed as previously described (8). The task was conducted on a white circular surface, 1.0 m in diameter, with 12 holes equally spaced around the perimeter (O′ Hara & Co., Tokyo, Japan). The training was performed 15 times before the probe test. A probe trial was conducted 24 h after the last training session. The time of latency to reach the target hole, number of errors, distance to reach the target hole and time spent around each hole were recorded using a video tracking software program (Time BCM; O′ Hara & Co.). To assess the long-term retention, a second probe trial was performed a week after the first probe test and an additional session of retraining.

Immunoblot analyses

Brains were homogenized in sample buffer (NaCl 150 mM, EDTA 1 mM, Tris–HCl 10 mM, 1% Triton X-100, 2% sodium dodecyl sulfate) and centrifuged at 15 000 rpm for 15 min. The protein concentration was measured by a BCA assay (Pierce, Rockford, IL, USA). The samples with DTT and sample buffer were separated by polyacrylamide gel electrophoresis on 10% NuPAGE Bis-Tris gels and transferred to polyvinylidene difluoride membranes. The membranes were probed with total asyn antibody (clone 42; BD Biosciences, Franklin Lakes, NJ, USA), phospho-specific asyn antibody (clone EP1536Y; Abcam, Cambridge, UK). They were visualized by standard immunoblot protocols using HRP-conjugated secondary antibodies (GE, Little Chalfont, UK; and eBioscience, Wien, Austria) and an ECL plus detection kit (GE). Band intensities were normalized to those of beta-actin (clone AC15; Sigma-Aldrich, St. Louis, MO, USA).

Immunohistochemistry

Mice were anesthetized with sevoflurane and transcardially perfused with cold phosphate-buffered saline (PBS). Dissected

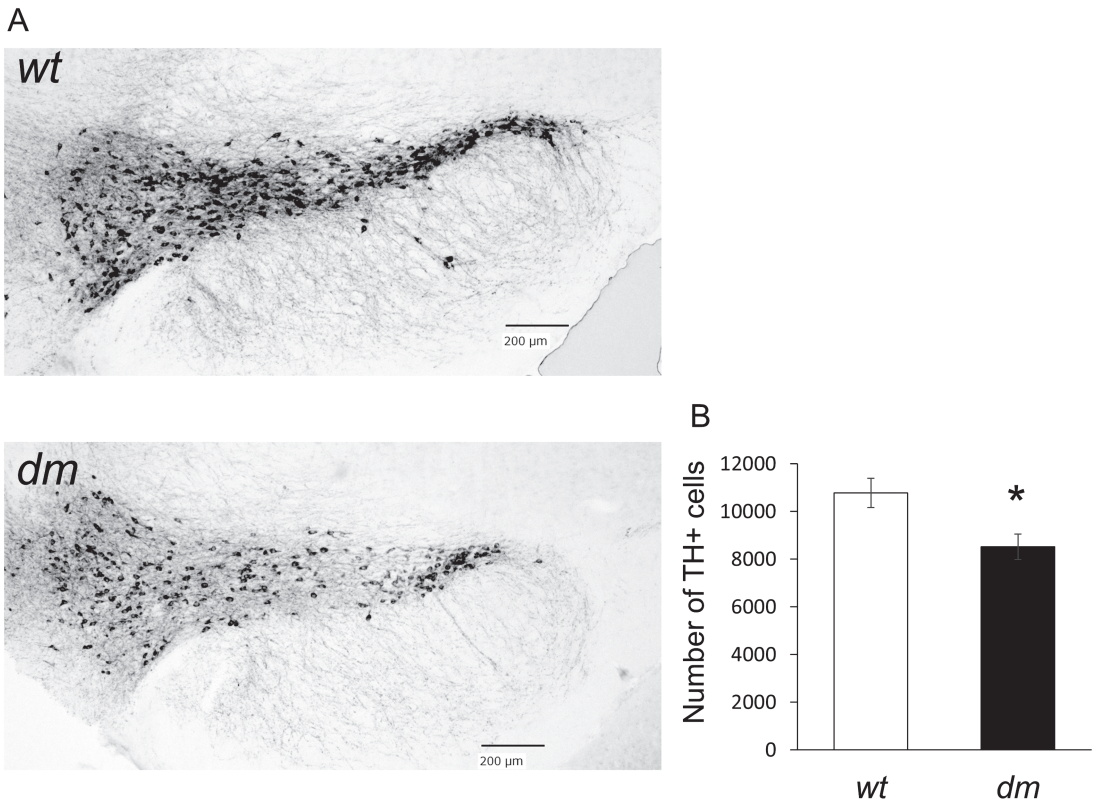

Figure 5. Number of TH-positive cells in SNpc was decreased in *dm* mice. (**A**) Representative immunohistochemical staining images for TH in the SNpc of *wt* mice and *dm* mice. (**B**) The number of TH-positive cells in the SNpc of *dm* mice was decreased compared to that of *wt* mice in 16- to 18-month-old. $n = 6$ for each genotype. The bars indicate mean ± SEM values. *: $P < 0.05$ by *t*-test. *wt*: wild type, *dm*: double-mutant, SNpc: substantia nigra pars compacta.

tissues were fixed with 4% paraformaldehyde in PBS at 4°C overnight. For vibratome sections, brains were cut to 40 μm thick sections (DSK, Kyoto, Japan). For paraffin embedded sections, brains were embedded onto paraffin and cut into 6 μm thick sections. The sections were incubated for 1 h in 5% goat serum blocking solution and then incubated with the primary antibody at 4°C overnight, reacted with a biotin-conjugated secondary antibody (Nichirei, Tokyo, Japan) and developed with 3,3′-diaminobenzidine (DAB) solution (KPL, Milford, MA, USA) using a Vectastain elite ABC kit (Vector Laboratories, Burlingame, CA, USA). The primary antibodies were the same as those used for western blotting and applied at a dilution of 1:500 to 1:2000.

Immunofluorescence staining

Mouse brains were obtained via the same method as for immunohistochemistry. Sections were obtained using a vibratome (DSK). The sections were incubated for 1 h in 5% goat serum blocking solution and then probed with a phospho-specific asyn antibody (clone EP1536Y; Abcam) and LAMP2 antibody (sc-18822; Santa Cruz Biotechnology, Dallas, TX, USA). The sections were then washed with PBS and treated with a secondary antibody.

Synaptic expression of asyn

Sections (40 μm) were obtained using a vibratome (DSK). Sections were permeabilized with 0.3% Triton X-100 in PBS (PBST) for 1 h and blocked with 10% normal goat serum in PBST for 12 h. Sections were then incubated with primary antibody in the blocking solution for 12 h. The sections were then washed with PBST and treated with a secondary antibody. For double immunostaining, this staining procedure was repeated. For the detection of asyn we used rabbit polyclonal antibody (sc-7011-R; Santa Cruz Biotechnology, Dallas, TX). This polyclonal antibody was visualized with Alexa594-conjugated secondary antibody (Molecular Probes, Eugene, OR, USA). Next, to detect the excitatory synapses, we used anti-vesicular glutamate transporter 1 (vGluT-1) guinea pig polyclonal antibody (AB5905; Millipore, Burlington, MA). This polyclonal antibody was visualized with fluorescein isothiocyanate-conjugated secondary antibody (Vector Laboratories). Sections were washed with PBST and then with 20 mM Tris–HCl buffer and mounted with FluorSave (Millipore). For confocal observation, images were acquired as Z stacks (10–20 z-sections, 1 μm apart, 1024 × 1024 pixels) using a Plan-Apochromat 63x/1.40 Oil DIC objective (Carl Zeiss, Oberkochen, Germany) with an inverted laser-scanning confocal microscope (LSM510; Carl Zeiss). Digital images obtained on the LSM510 were processed using the software program Adobe Photoshop 7.0 (Adobe, San Jose, CA). Each image was processed equally between *wt* mouse-derived and *tg* mouse-derived specimens.

Semithin sections and EM

Animal anesthetization, fixation and tissue processing for conventional EM and pre-embedding immunoelectron microscopy were performed as described previously (29), with some modifications. For conventional EM, 19-month-old *dm* and littermate *wt* mice ($n = 2$) were deeply anesthetized and perfused with 100 ml of fixative containing 2% paraformaldehyde and 2%

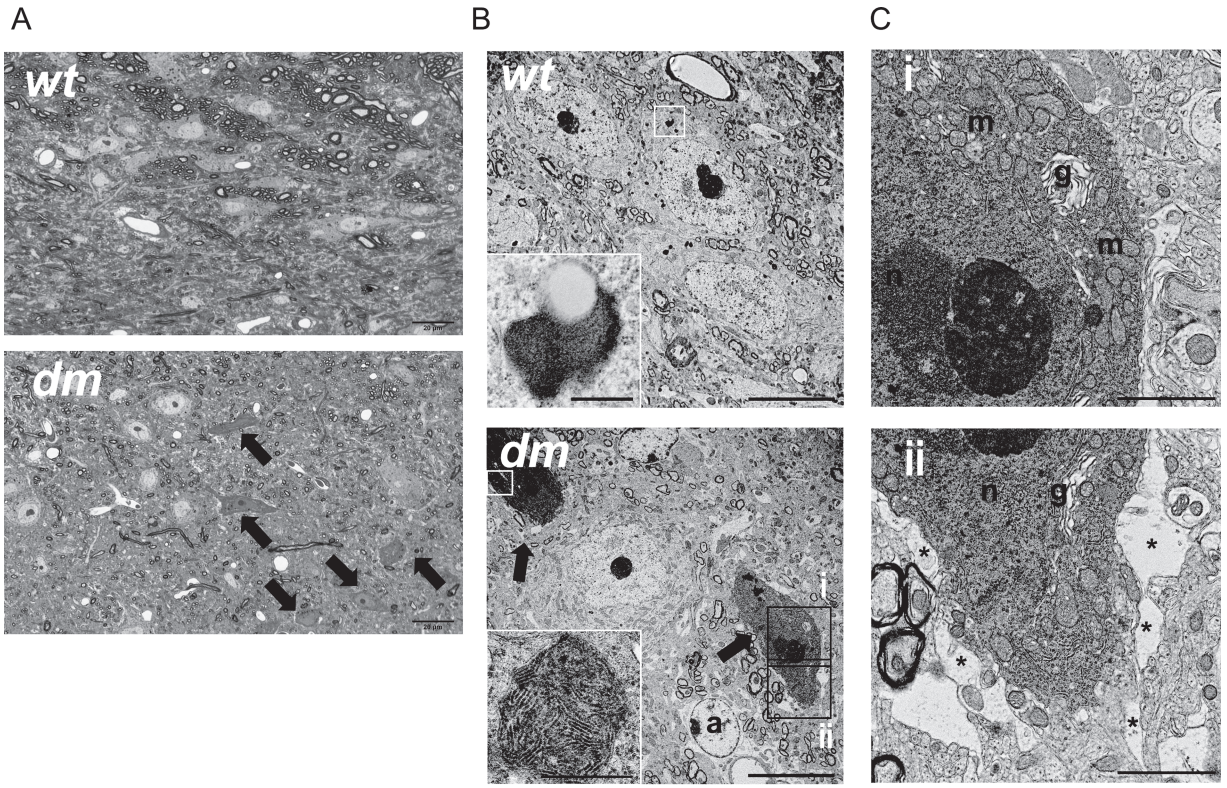

Figure 6. Nigral neurodegeneration in *dm* mice. (**A**) Semithin sections of SNpc from 19-month-old mice. In *dm* mice, massive shrinking neurons were visible (arrows). Bars indicate 20 µm. (**B**) EM of the neurons in SNpc from 19-month-old mice. In *dm* mice, degenerating neurons with a high electron density were observed (arrows). Note that membranous structures were accumulated in the lipofuscins of neurons in *dm* mice (white inset). The bars indicate 10 µm (500 nm in white insets). (**C**) Magnification of the black boxes in (B). The accumulation of mitochondria (m) and vacuolation of the Golgi apparatus (g) were seen in the perikarya. Degenerating neurons were surrounded by electro-lucent processes (asterisks), possibly derived from astrocytes (a). The bars indicate 2 µm. n: nucleus, *wt*: wild type, *dm*: double-mutant, SNpc: substantia nigra pars compacta.

glutaraldehyde in 0.1 M cacodylate buffer (pH 7.2). The brains were removed from the skull immediately after perfusion, post-fixed in the same fixative and coronally sectioned at 100 µm using a slicer (Linear Slicer Pro7; Dosaka EM, Kyoto, Japan). The sections were post-fixed in 1% osmium tetroxide, counterstained for 35 min with 1% uranyl acetate and dehydrated in graded ethanol series for 10 min each. Following 10 min incubation in propylene oxide, the sections were infiltrated overnight in Durcapan resin (Sigma-Aldrich) and flat-embedded in a glass slide at 60°C for 2 nights for resin curing. Semithin sections were cut at 1 µm with a Leica UC7 ultramicrotome (Leica Microsystems, Wetzlar, Germany) and stained with toluidine blue. For EM, silver sections were cut with an ultramicrotome, stained with uranyl acetate and lead citrate and observed with a Hitachi HT7700 electron microscope (Hitachi, Tokyo, Japan).

For pre-embedding immunoelectron microscopy, 19-month-old *dm* mice and littermate *wt* mice ($n = 2$) were deeply anesthetized and perfused with 100 ml of fixative containing 4% paraformaldehyde and 0.05% glutaraldehyde in 0.1 M phosphate buffer (pH 7.2). The brains were removed from the skull immediately after perfusion, post-fixed in 4% paraformaldehyde overnight at 4°C and coronally sectioned at 50 µm by a slicer (Linear Slicer Pro7; Dosaka EM). The sections were cryoprotected, freeze-thawed and blocked for 1 h at room temperature in blocking solution containing 20% normal goat serum in 50 mM tris-buffer saline (TBS) containing 0.03% Triton X-100. The sections were incubated for 4 nights in anti-total asyn antibody (clone 42; BD Biosciences) at a concentration of 1 µg/ml and 1 night in anti-mouse secondary antibody conjugated to 1.4 nm gold particles (Nanoprobes, Yaphank, NY, USA). The sections were then fixed in 1% glutaraldehyde. Following several washes in TBS and water, the sections were incubated using a Nanoprobes HQ silver enhancement kit. The sections were post-fixed in 1% osmium tetroxide, counterstained for 35 min with 1% uranyl acetate and flat-embedded in Durcapan resin as mentioned above. Approximately 70 nm thick ultrathin sections were cut from the external plexiform layer of the Ob, stained briefly with 1% uranyl acetate and 1% lead citrate, and observed with a Hitachi HT7700 electron microscope.

Counting TH-positive cells in the SNpc

Sections (40 µm) were prepared from coronally dissected frozen tissues of mouse midbrain. The sections were immunostained with anti-TH antibody (AB152; Millipore). The numbers of TH-positive neurons of each genotype were then counted using a stereology technique (MBF Bioscience, Williston, VT, USA) ($n = 6$) (30).

GBA activity

Brain tissues were homogenized in 4 µl/mg sample buffer (10 mM Tris-HCl at pH 7.4, 150 mM NaCl, 1% Triton X-100) followed by sonication and centrifugation (15 000 rpm; 5 min, 4°C). Reaction solution was made by mixing 7 mM 4-methylumbelliferyl-

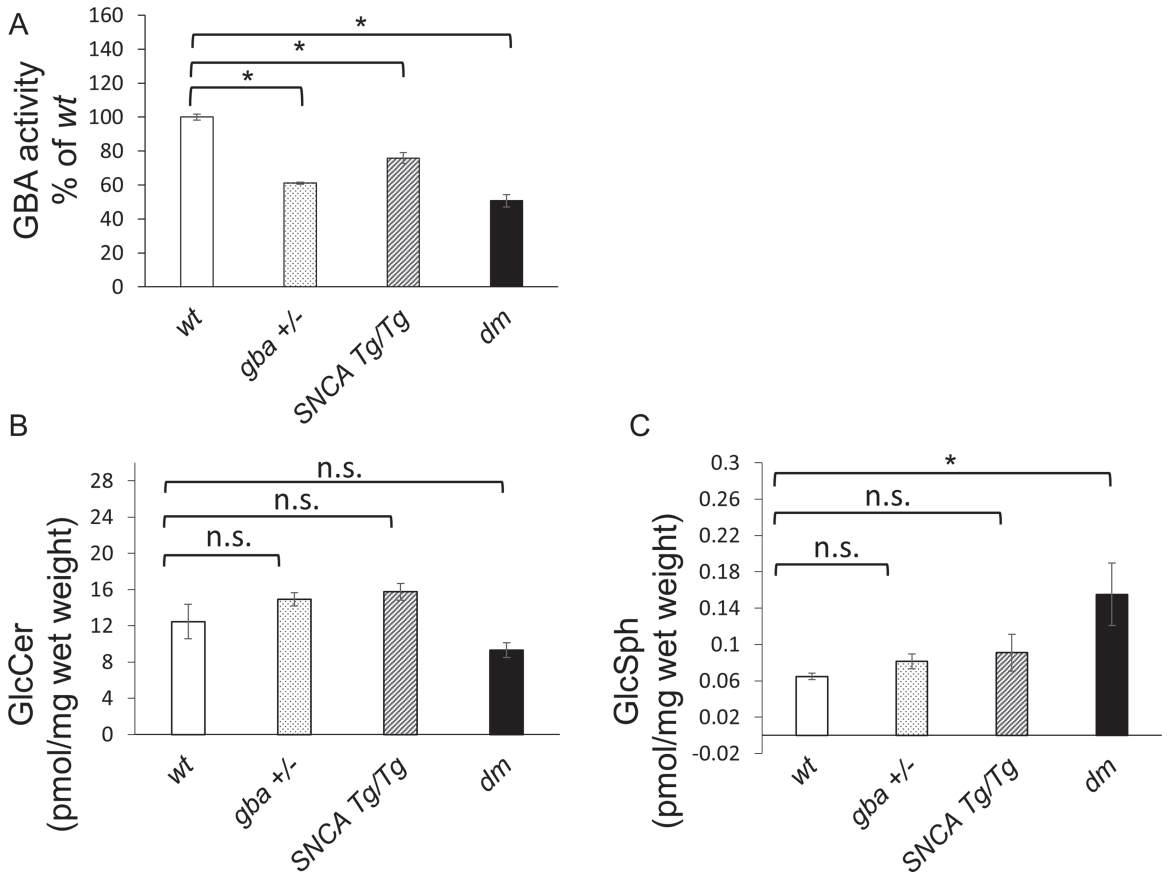

Figure 7. Reduction in the GBA activity and the accumulation of glucosylsphingosine (GlcSph) in *dm* mice. (**A**) The GBA activity of whole brain homogenates in 8-month-old mice. The GBA activity was also significantly decreased in asyn *tg* +/+ mice without *gba* mutation ($P < 0.05$) and was lowest in *dm* mice. $n = 3$ for each genotype. (**B**) An analysis of glucosylceramide (GlcCer) in the cerebral cortex of 15-month-old mice. The amount of GlcCer was not significantly increased in *dm* mice. $n = 4$ for *wt* mice, $n = 6$ for other genotypes. (**C**) An analysis of glucosylsphingosine (GlcSph) in the cerebral cortex of 15-month-old mice. GlcSph was significantly accumulated in *dm* mice. $n = 4$ for *wt* mice, $n = 6$ for other genotypes. The bars indicate the mean ± SEM values in all graphs. *wt*: wild type, *dm*: double-mutant. $^*P < 0.05$ by Dunnett's multiple comparison test.

β-D-glucopyranoside solution, 20% (w/v) taurocholate solution and water at a ratio of 7:0.5:1. For the negative control, 20 mM conduritol B epoxide (CBE) solution was used instead of water. Sample solution (15 µl) and 85 µl of reaction solution were mixed and incubated at 37°C for 30 min. The reaction was stopped by adding 100 µl of 0.4 M glycine. The product of the enzymatic reaction (4-methylumbelliferone) was measured fluorometrically at pH 10.3 with excitation at 365 nm and emission at 445 nm. For each sample, the differences in the fluorescence values between those with or without CBE were estimated to be proportional to the GBA activity.

Glycolipids related to GBA

β-D-Glucopyranosyl-(1 → 1)-N-lauroyl-D-erythro-sphingosine (GlcCer [d18:1-C12:0]) and β-D-glucopyranosyl-(1 → 1)-D-erythro-sphingosine-d5 (GlcSph-d5) were purchased from Avanti Polar Lipids (Alabaster, AL, USA). For liquid chromatography (LC)-ESI-MS/MS, high-performance LC-grade acetonitrile and methanol were purchased from Thermo Fisher Scientific (Waltham, MA, USA), chloroform and distilled water from Kanto Chemical Co., Inc. (Tokyo, Japan) and ammonium formate from Sigma-Aldrich Japan.

The frozen tissue (~50 mg) was homogenized, and total lipids were extracted with a chloroform:methanol (C:M) (2:1 [v/v], 5 ml) mixture spiked with 1 pmol/mg frozen tissue of GlcCer (d18:1-C12:0) and GlcSph-d5 each as internal standards. Extracts were dried under a flow of N_2 gas and hydrolyzed for 2 h at room temperature in C:M (2:1 [v/v], 2 ml) containing 0.1 M KOH. After neutralization with 7.5 µl of glacial acetic acid, the reaction mixture was subjected to Folch's partition and the lower phase was dried under a flow of N_2 gas. The resulting lipid film was suspended in C:M (2:1, v/v) at a concentration of 100 µg frozen tissue/µl, and aliquots were subjected to an LC-ESI-MS/MS analysis.

The LC-ESI-MS/MS analysis was performed on an LC system Nexera X2 (SHIMADZU, Kyoto, Japan) fused to a triple quadrupole linear ion trap mass spectrometer, QTRAP4500 (SCIEX, Tokyo, Japan). The datasets were analyzed with the MultiQuant and Analyst software programs (SCIEX). Target lipids were monitored in multiple reaction monitoring (MRM) mode using specific precursor–product ion pairs, as detailed in Supplementary Material, Table S1. Peak areas were integrated and quantified relative to the associated internal standard.

GlcCer was analyzed as previously reported by HILIC-ESI-MS/MS with minor modifications. In brief, 100 µg frozen tissue/µl of the lipid extracts was diluted 10-fold with mobile phase A (acetonitrile:methanol:formic acid, 97:2:1 [v/v/v], with 5 mM ammonium formate), and aliquots (10 µl) were applied to an Atlantis silica HILIC column (2.1 mm inner diameter × 150 mm,

particle size, 3 μm; Waters, Milford, MA, USA) maintained at 40°C. Samples were eluted at a flow rate of 0.05 ml/min, utilizing the following gradient of mobile phase B (methanol:water:formic acid, 89:9:1 [v/v/v], with 20 mM ammonium formate): 3.3 min, 0%; 23.4 min, 0–35% linear gradient; 1.3 min, 35–70% linear gradient, 0.05–0.15 ml/min linear gradient flow rate; 8 min, 70% (washing step); 29 min, 0%, flow rate increased to 0.2 ml/min (equilibration); 2 min, 0%, flow rate decreased to 0.05 ml/min. The mass spectrometer was set to positive ion mode (ion spray voltage, 5500 V; curtain gas pressure, 30 psi; nebulizer gas pressure, 90 psi; heating gas pressure, 30 psi, temperature, 100°C) utilizing MRM detection for a targeted analysis. The quantitative values of GlcCer with various chain lengths of fatty acids (C16:0, C18:0, C20:0, C22:0, C23:0, C24:1 and C24:0) were summarized.

Similar to GlcCer, GlcSph was analyzed by HILIC-ESI-MS/MS with minor modifications. Samples were eluted at a flow rate of 0.15 ml/min, utilizing the following gradient of mobile phase B: 3.3 min, 0%; 13.4 min, 0–35% linear gradient; 1.3 min, 35–70% linear gradient; 3 min, 70% (washing step); 30 min, 0%, flow rate increased to 0.2 ml/min (equilibration). The mass spectrometer was set to positive ion mode (ion spray voltage, 5500 V; curtain gas pressure, 20 psi; nebulizer gas pressure, 70 psi; heating gas pressure, 80 psi, temperature, 700°C) utilizing MRM detection for a targeted analysis.

Ceramide and D-erythro-sphingosine (d18:1-sphingosine) were analyzed by reversed-phase LC-ESI-MS/MS. The lipid extracts dissolved in C:M (2:1, v/v) were diluted 10-fold with mobile phase B (M:W 85:15 [v/v], 5 mM ammonium acetate) and applied to an RP column (Luna C18 (2) column; 2 mm inner diameter × 250 mm, particle size, 3 μm; Phenomenex, Torrance, CA, USA) maintained at 36°C and at a flow rate of 0.15 ml/min. The samples were then eluted with the following gradients of mobile phase A (methanol pure, 5 mM ammonium acetate): 2 min, 0%; 13 min, 0–100% linear gradient; 40 min, 100% (washing step); 15 min 0% (equilibration). The mass spectrometer was set to positive ion mode (ion spray voltage, 5500 V; curtain gas pressure, 40 psi; nebulizer gas pressure, 70 psi; heating gas pressure, 80 psi, temperature, 600°C), utilizing either MRM detection for a targeted analysis. The quantitative values of ceramide with various chain lengths of fatty acids (C16:0, C18:0, C20:0, C22:0, C23:0, C24:1 and C24:0) were summarized.

Statistical analyses

Statistical analyses were carried out using the Graphpad Prism software program, version 5.04 (MDF, Tokyo, Japan). The significance of differences between two groups was analyzed by an unpaired t-test, with $P < 0.05$ deemed significant. The significance of changes between four groups or more were analyzed by a one-way analysis of variance, followed by Tukey's multiple comparison test for immunoblot and Dunnett's multiple comparison test for other analyses, with $P < 0.05$ deemed significant.

Supplementary Material

Supplementary Material is available at *HMG* online.

Acknowledgements

We thank Ms. Rie Hikawa and Mr. Ryutaro Tamano for the technical support.

Conflict of Interest statement. None declared.

Funding

Brain/MINDS from MEXT and AMED (JP15dm0207020 and JP15dm0207024); Grants-in-Aid for Scientific Research (A) (JP18H04041); CREST, JST (JP18gm0710011).

References

1. Chartier-Harlin, M.C., Kachergus, J., Roumier, C., Mouroux, V., Douay, X., Lincoln, S., Levecque, C., Larvor, L., Andrieux, J., Hulihan, M. *et al.* (2004) Alpha-synuclein locus duplication as a cause of familial Parkinson's disease. *Lancet*, **364**, 1167–1169.
2. Ibanez, P., Bonnet, A.M., Debarges, B., Lohmann, E., Tison, F., Pollak, P., Agid, Y., Durr, A. and Brice, A. (2004) Causal relation between alpha-synuclein gene duplication and familial Parkinson's disease. *Lancet*, **364**, 1169–1171.
3. Singleton, A.B., Farrer, M., Johnson, J., Singleton, A., Hague, S., Kachergus, J., Hulihan, M., Peuralinna, T., Dutra, A., Nussbaum, R. *et al.* (2003) alpha-synuclein locus triplication causes Parkinson's disease. *Science*, **302**, 841.
4. Simon-Sanchez, J., Schulte, C., Bras, J.M., Sharma, M., Gibbs, J.R., Berg, D., Paisan-Ruiz, C., Lichtner, P., Scholz, S.W., Hernandez, D.G. *et al.* (2009) Genome-wide association study reveals genetic risk underlying Parkinson's disease. *Nat. Genet.*, **41**, 1308–1312.
5. Satake, W., Nakabayashi, Y., Mizuta, I., Hirota, Y., Ito, C., Kubo, M., Kawaguchi, T., Tsunoda, T., Watanabe, M., Takeda, A. *et al.* (2009) Genome-wide association study identifies common variants at four loci as genetic risk factors for Parkinson's disease. *Nat. Genet.*, **41**, 1303–1307.
6. Feany, M.B. and Bender, W.W. (2000) A Drosophila model of Parkinson's disease. *Nature*, **404**, 394–398.
7. Giasson, B.I., Duda, J.E., Quinn, S.M., Zhang, B., Trojanowski, J.Q. and Lee, V.M. (2002) Neuronal alpha-synucleinopathy with severe movement disorder in mice expressing A53T human alpha-synuclein. *Neuron*, **34**, 521–533.
8. Yamakado, H., Moriwaki, Y., Yamasaki, N., Miyakawa, T., Kurisu, J., Uemura, K., Inoue, H., Takahashi, M. and Takahashi, R. (2012) alpha-synuclein BAC transgenic mice as a model for Parkinson's disease manifested decreased anxiety-like behavior and hyperlocomotion. *Neurosci. Res.*, **73**, 173–177.
9. Sidransky, E., Nalls, M.A., Aasly, J.O., Aharon-Peretz, J., Annesi, G., Barbosa, E.R., Bar-Shira, A., Berg, D., Bras, J., Brice, A. *et al.* (2009) Multicenter analysis of glucocerebrosidase mutations in Parkinson's disease. *N. Engl. J. Med.*, **361**, 1651–1661.
10. Xu, Y.H., Sun, Y., Ran, H., Quinn, B., Witte, D. and Grabowski, G.A. (2011) Accumulation and distribution of alpha-synuclein and ubiquitin in the CNS of Gaucher disease mouse models. *Mol. Genet. Metab.*, **102**, 436–447.
11. Cullen, V., Sardi, S.P., Ng, J., Xu, Y.H., Sun, Y., Tomlinson, J.J., Kolodziej, P., Kahn, I., Saftig, P., Woulfe, J. *et al.* (2011) Acid beta-glucosidase mutants linked to Gaucher disease, Parkinson disease, and Lewy body dementia alter alpha-synuclein processing. *Ann. Neurol.*, **69**, 940–953.
12. Taguchi, Y.V., Liu, J., Ruan, J., Pacheco, J., Zhang, X., Abbasi, J., Keutzer, J., Mistry, P.K. and Chandra, S.S. (2017) Glucosylsphingosine promotes alpha-synuclein pathology in mutant GBA-associated Parkinson's disease. *J. Neurosci.*, **37**, 9617–9631.

13. Cheng, F., Vivacqua, G. and Yu, S. (2011) The role of alpha-synuclein in neurotransmission and synaptic plasticity. *J. Chem. Neuroanat.*, **42**, 242–248.
14. Braak, H., Del Tredici, K., Rub, U., de Vos, R.A., Jansen Steur, E.N. and Braak, E. (2003) Staging of brain pathology related to sporadic Parkinson's disease. *Neurobiol. Aging.*, **24**, 197–211.
15. Fujiwara, H., Hasegawa, M., Dohmae, N., Kawashima, A., Masliah, E., Goldberg, M.S., Shen, J., Takio, K. and Iwatsubo, T. (2002) alpha-synuclein is phosphorylated in synucleinopathy lesions. *Nat. Cell. Biol.*, **4**, 160–164.
16. Turmaine, M., Raza, A., Mahal, A., Mangiarini, L., Bates, G.P. and Davies, S.W. (2000) Nonapoptotic neurodegeneration in a transgenic mouse model of Huntington's disease. *Proc. Natl. Acad. Sci. U. S. A.*, **97**, 8093–8097.
17. Xu, Y.H., Quinn, B., Witte, D. and Grabowski, G.A. (2003) Viable mouse models of acid beta-glucosidase deficiency: the defect in Gaucher disease. *Am. J. Pathol.*, **163**, 2093–2101.
18. Migdalska-Richards, A. and Schapira, A.H. (2016) The relationship between glucocerebrosidase mutations and Parkinson disease. *J. Neurochem.*, **139**(Suppl 1), 77–90.
19. Gan-Or, Z., Giladi, N., Rozovski, U., Shifrin, C., Rosner, S., Gurevich, T., Bar-Shira, A. and Orr-Urtreger, A. (2008) Genotype–phenotype correlations between GBA mutations and Parkinson disease risk and onset. *Neurology*, **70**, 2277–2283.
20. Unger, E.L., Eve, D.J., Perez, X.A., Reichenbach, D.K., Xu, Y., Lee, M.K. and Andrews, A.M. (2006) Locomotor hyperactivity and alterations in dopamine neurotransmission are associated with overexpression of A53T mutant human alpha-synuclein in mice. *Neurobiol. Dis.*, **21**, 431–443.
21. Mazzulli, J.R., Xu, Y.H., Sun, Y., Knight, A.L., McLean, P.J., Caldwell, G.A., Sidransky, E., Grabowski, G.A. and Krainc, D. (2011) Gaucher disease glucocerebrosidase and alpha-synuclein form a bidirectional pathogenic loop in synucleinopathies. *Cell*, **146**, 37–52.
22. Fishbein, I., Kuo, Y.M., Giasson, B.I. and Nussbaum, R.L. (2014) Augmentation of phenotype in a transgenic Parkinson mouse heterozygous for a Gaucher mutation. *Brain*, **137**, 3235–3247.
23. Nilsson, O. and Svennerholm, L. (1982) Accumulation of glucosylceramide and glucosylsphingosine (psychosine) in cerebrum and cerebellum in infantile and juvenile Gaucher disease. *J. Neurochem.*, **39**, 709–718.
24. Zunke, F., Moise, A.C., Belur, N.R., Gelyana, E., Stojkovska, I., Dzaferbegovic, H., Toker, N.J., Jeon, S., Fredriksen, K. and Mazzulli, J.R. (2018) Reversible conformational conversion of alpha-synuclein into toxic assemblies by glucosylceramide. *Neuron*, **97**, 92–107.
25. Tayebi, N., Parisiadou, L., Berhe, B., Gonzalez, A.N., Serra-Vinardell, J., Tamargo, R.J., Maniwang, E., Sorrentino, Z., Fujiwara, H., Grey, R.J. *et al.* (2017) Glucocerebrosidase haploinsufficiency in A53T alpha-synuclein mice impacts disease onset and course. *Mol. Genet. Metab.*, **122**, 198–208.
26. Gegg, M.E., Burke, D., Heales, S.J., Cooper, J.M., Hardy, J., Wood, N.W. and Schapira, A.H. (2012) Glucocerebrosidase deficiency in substantia nigra of Parkinson disease brains. *Ann. Neurol.*, **72**, 455–463.
27. Tybulewicz, V.L., Tremblay, M.L., LaMarca, M.E., Willemsen, R., Stubblefield, B.K., Winfield, S., Zablocka, B., Sidransky, E., Martin, B.M., Huang, S.P. *et al.* (1992) Animal model of Gaucher's disease from targeted disruption of the mouse glucocerebrosidase gene. *Nature*, **357**, 407–410.
28. Uemura, M.T., Asano, T., Hikawa, R., Yamakado, H. and Takahashi, R. (2017) Zonisamide inhibits monoamine oxidase and enhances motor performance and social activity. *Neurosci. Res.*, **124**, 25–32.
29. Parajuli, L.K., Nakajima, C., Kulik, A., Matsui, K., Schneider, T., Shigemoto, R. and Fukazawa, Y. (2012) Quantitative regional and ultrastructural localization of the Ca(v)2.3 subunit of R-type calcium channel in mouse brain. *J. Neurosci.*, **32**, 13555–13567.
30. Wang, H.Q., Imai, Y., Inoue, H., Kataoka, A., Iita, S., Nukina, N. and Takahashi, R. (2008) Pael-R transgenic mice crossed with parkin deficient mice displayed progressive and selective catecholaminergic neuronal loss. *J. Neurochem.*, **107**, 171–185.